



# New Insight into the Pharmacological Importance of Atropine as the Potential Inhibitor of AKR1B1 via Detailed Computational Investigations: DFTs, ADMET, Molecular Docking, and Molecular Dynamics Studies

Syeda Abida Ejaz<sup>1</sup> · Mubashir Aziz<sup>1</sup> · Aftab Ahmed<sup>1</sup> · Saqer S. Alotaibi<sup>2</sup> · Sarah M. Albogami<sup>2</sup> · Farhan Siddique<sup>3,4</sup> · Gaber El-Saber Batiha<sup>5</sup>

Accepted: 17 February 2023 / Published online: 27 February 2023  
© The Author(s), under exclusive licence to Springer Science+Business Media, LLC, part of Springer Nature 2023

## Abstract

The aim of this research is to investigate the quantum geometric properties and chemical reactivity of atropine, a pharmaceutically active tropane alkaloid. Using density functional theory (DFT) computations with the B3LYP/SVP functional theory basis set, the most stable geometry of atropine was determined. Additionally, a variety of energetic molecular parameters were calculated, such as the optimized energy, atomic charges, dipole moment, frontier molecular orbital energies, HOMO–LUMO energy gap, molecular electrostatic potential, chemical reactivity descriptors, and molecular polarizability. To determine atropine's inhibitory potential, molecular docking was used to analyze ligand interactions within the active pockets of aldo–keto reductase (AKR1B1 and AKR1B10). The results of these studies showed that atropine has greater inhibitory action against AKR1B1 than AKR1B10, which was further validated through molecular dynamic simulations by analyzing root mean square deviation (RMSD) and root mean square fluctuations (RMSF). The results of the molecular docking simulation were supplemented with simulation data, and the ADMET characteristics were also determined to predict the drug likeness of a potential compound. In conclusion, the research suggests that atropine has potential as an inhibitor of AKR1B1 and could be used as a parent compound for the synthesis of more potent leads for the treatment of colon cancer associated with the sudden expression of AKR1B1.

**Keywords** Tropane alkaloid · Chemical reactivity descriptors · Aldo–keto reductase · Molecular docking

## Introduction

The third most common cancer in the world causing high proportion of cancer-related deaths is colon cancer [1]. Aldo–keto reductases (AKR1B1 and AKR1B10) are a group of enzymes which has been found highly upregulated in colon cancer. It has been

---

✉ Syeda Abida Ejaz  
abida.ejaz@iub.edu.pk; abidaejaz2010@gmail.com

Extended author information available on the last page of the article

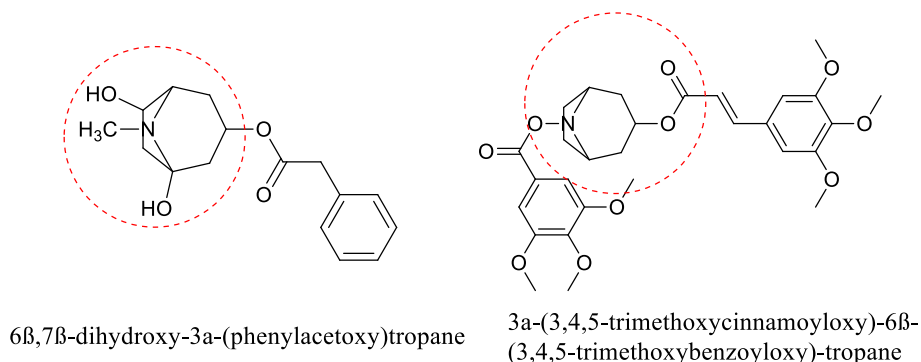


**Fig. 1** Illustration of already reported anticancer tropane alkaloids [14]

demonstrated earlier that the elevated expression of AKR1B1 is associated with higher mortality, inflammation, aberrant metabolic pathway activation, and poor clinical outcome in colon cancer [2]. Another member of AKR family, i.e., AKR1B10, shares 71% structural resemblance with AKR1B1 [3, 4]. The enzymes AKR1B1 and AKR1B10 use NADPH as a cofactor to reduce a variety of aromatic and aliphatic aldehydes, dicarbonyl compounds, and certain drug ketones [4–6]. Hence, by targeting the AKR1B1, colon cancer and its associated malignancies can be treated.

Plant alkaloids, which are considered one of the largest groups of secondary metabolites, contain an almost 12000 natural chemical compounds plant [7]. These are well known for their immense biological properties playing a vital role in human life [8]. They have a great deal of medicinal significance and are used to treat a variety of lethal conditions, including cancer. These secondary metabolites have a wide range of biological properties including muscle relaxant, antioxidant, anticancer, anti-inflammatory, antibacterial, and amoebicidal activity, among others [9, 10].

Among the various secondary metabolites, tropane alkaloids are among the world's earliest compounds known in medicine. These are the active constituents obtained from various poisonous plants and are alkaline in nature, with atropine identified from *Atropa belladonna* L. Atropine is an enantiomeric mixture of d-hyoscyamine and l-hyoscyamine, and most of the physiological activities are due to l-hyoscyamine. The major pharmacological action of tropane alkaloids is significant pupil dilation (mydriasis), followed by lens accommodation impairment (cycloplegia). A common tropane alkaloid and preferred drug for ophthalmologic applications due to its significant anticholinergic properties is atropine [11]. Atropine is associated with lesser side effects on the central nervous system than its comparative drug hyoscyamine with more stability and easy standardization. Additionally, it suppresses respiratory tract secretions and bronchodilator and also induces bradycardia at low doses while tachycardia is the result of high dose [12]. The side effect of atropine includes decreased gastric secretions and hyperthermia associated with no sweating. Atropine is also used as a standard antidote in poisoning caused by organic phosphorus compounds (insecticides). Already reported tropanes have anti-proliferative activity, i.e., 6β,7β-dihydroxy-3α-(phenylacetoxyl)tropane [5] and 3α-(3,4,5-trimethoxycinnamoyloxy)-6β-(3,4,5-trimethoxybenzoyloxy)-tropane [6], and their structures are shown in Fig. 1. The l-enantiomer of atropine is believed to have more activity in terms of its pharmacological effects as compared to the d-enantiomer [13]. This is because the l-enantiomer is able to

bind to and effectively block the activity of the muscarinic acetylcholine receptors in the body, which are responsible for mediating many of the physiological effects of atropine. In contrast, the *d*-enantiomer does not bind as effectively to these receptors and thus has less activity.

Targeting AKR1B1 and AKR1B10 with atropine is a novel approach in the field of drug development. AKR1B1 and AKR1B10 are enzymes that are involved in the metabolism of various compounds and have been linked to various diseases including cancer. The overexpression of these enzymes has been associated with poor prognosis and resistance to chemotherapy. Traditional approaches to target these enzymes have focused on the development of specific inhibitors; however, atropine, a tropane alkaloid, has been found to have a strong binding affinity and inhibition potential towards AKR1B1 and AKR1B10. The use of atropine as an inhibitor of these enzymes has the potential to offer a new avenue for the treatment of diseases associated with their overexpression. Additionally, atropine has a lower toxicity level compared to other compounds and it is also used as a standard antidote in poisoning caused by organic phosphorus compounds (insecticides). This makes atropine as a promising candidate for the development of new drugs for the treatment of conditions associated with the overexpression of AKR1B1 and AKR1B10.

This study aims to identify the aldo–keto reductase inhibitory potential of atropine (*l*-enantiomer) using various computation tools, i.e., density functional theory, molecular docking, and molecular dynamic simulations. DFT calculations are standardized method for obtaining information about the structure optimization and electronic characteristics of molecules. B3LYP is a well-known hybrid functional theory that is used to investigate electronic structure, atomic spectra, and various quantum characteristics of molecules. DFT study is an efficient method as compared to other quantum chemistry approaches due to its reliable precision, low processing cost, and high predictability [15]. Quantum chemistry calculations are primarily concerned with determining the most stable molecular geometry with lowest energy, which is then utilized to collect molecular spectra and various other energy parameters to confirm the compound's structure. The study also includes various quantum chemical descriptors in addition to HOMO and LUMO energies, molecule polarizability, and reactivity prediction based on LUMO/HOMO energy transitions [16]. The binding energy of atropine in the active pocket of AKR1B1 and AKR1B10 was determined using molecular docking. Molecular docking is most commonly used computation method in current drug discovery because of reliable prediction of the ligand bonding. Using MD simulations, in-depth understanding of stability and viability of binding mechanisms of the compounds can be analyzed. ADMET characteristics were also calculated to determine the compound's drug likeness properties [15, 17].

## Methodology

### Density Functional Theory Studies

Following the geometric optimization, the stereo-structural forms of the chosen molecule were calculated using density functional theory (DFT) with the Gaussian 09w software [18]. To ensure high precision, the SVP basis set was utilized in this work [19]. The best exchange–correlation function chosen was the B3LYP hybrid functional [20]. To view and check the files, GaussView 06 was used [21]. The molecular geometry was optimized by minimizing the electronic energy of the molecule using the DFT method until the

convergence criteria were met (maximum force acting on each atom was less than 0.0001 Hartree/bohr and the maximum change in energy was less than 0.0001 Hartree) [22]. Once the geometry was optimized, the harmonic vibrational frequencies were calculated to confirm that the optimized structure corresponds to a minimum on the potential energy surface. The thermal correction for the zero-point energy (ZPE) was added to the optimized electronic energy, and the Gibbs free energy was calculated at different temperatures using the harmonic vibrational frequency analysis. The thermodynamic properties like enthalpy, entropy, and heat capacity, were calculated from the Gibbs free energy values at different temperatures [23].

### Preparation of Ligand

Prior to docking, the ligand molecule was orientated and adjusted for energy minimization in Chem 3D Pro 12.0 [24] and then imported in the required SDF format [25].

### Preparation of Protein

The aldo–keto reductases AKR1B1 and AKR1B10 were selected as enzyme targets for this investigation, and their crystal structures in PDB formats were obtained from the Protein Data Bank ([www.rcsb.com](http://www.rcsb.com) assessed on 1–8-2022) [26] with the PDB IDs 6F7R and 4GQG for AKR1B1 and AKR1B10, respectively. The 6F7R was selected for AKR1B1 due to its high resolution of 0.92 Å. In addition, 4GQG was used to retrieve AKR1B10 due to its resolution of 1.92 Å which is quite good. Furthermore, complexation with substrate molecule and improved experimental screen shot was the reason for choosing the specified structure. Initially, water molecules and heteroatoms were eliminated from the protein using MGL tools [27]. After that, polar hydrogen atoms were integrated into the protein. The protein was also incorporated with gasteiger charges and any missing residues were fixed.

### Docking Protocol

Docking simulations were carried out using AutoDock Vina software [28]. The grid box dimensions of the co-crystal ligand were used for the docking process. For AKR1B1, the grid box dimensions were  $x = +3.845357$ ,  $y = -8.840679$ , and  $z = +10.758179$ , with center size of 40, 40, and 40 in  $x$ ,  $y$ , and  $z$  dimensions. Similarly, for AKR1B10, the grid box dimensions were  $x = -2.559852$ ,  $y = +25.087000$ , and  $z = -5.933593$ , with center size of 40, 40, and 40 in  $x$ ,  $y$ , and  $z$  dimensions respectively [29]. An exhaustiveness value of 10 was used for the docking process to ensure a thorough search for the best-docked conformation. Epalrestat was used as a standard inhibitor and docked alongside the co-crystal ligand and atropine to validate the docking process. This method was used to predict the binding mode and binding energy of the compounds in the active site of AKR1B1 and AKR1B10 [30].

The docking process was initiated by carefully configuring the grid box in AutoDock. The size of the selected grid box was set to 40, 40, and 40 and a grid point spacing of 0.375 Å was used in the  $x$ ,  $y$ , and  $z$  dimensions. A GPF (grid parameter file) was created to assist AutoGrid in retrieving the map files. A population size of 150 and a limit of 100 GA (genetic algorithm) runs were used. The Lamarckian genetic algorithm (LGA) [31] was employed to determine the sampling power. The default scoring function was used to

determine the pose of the ligand in the binding site of the receptor. In addition, exhaustiveness was set to the default value of 8 which had provided efficient results. The use of these parameters and methods ensured a thorough and accurate search for the best-docked conformation and the best-binding energy of the compounds in the active site of AKR1B1 and AKR1B10 [32].

## Visualization

The generated poses from AutoDock Vina were analyzed using the Discovery Studio Visualizer software. This software allows for the visualization of the docked poses in 3D, and provides various tools for the analysis and interpretation of the results. The generated poses were analyzed for their binding modes and binding energies, as well as their interactions with the active site residues of AKR1B1 and AKR1B10. This analysis was done in order to understand the mechanism of inhibition and the key interactions that contribute to the binding of atropine to the enzymes [33].

## Validation

The docking protocol was validated through redocking of co-crystal ligand at active site; the RMSD value of less than 2 Å between native pose and regenerated pose was considered validated molecular docking approach [34].

## Molecular Dynamic Simulation

The molecular dynamic simulations were carried out according to the procedure detailed in our previous article [35]. Desmond, a software package from Schrödinger LLC [36], was utilized to simulate molecular dynamics for 100 ns. [37] Detailed protocols for protein preparation and NPT equilibration [38] can be found in the supplementary file.

## ADMET Properties

To anticipate a compound's drug likeness, ADMET properties such as absorption, distribution, metabolism, excretion, and toxicity are evaluated. All of the above-mentioned features were examined in the way described in our earlier article [39]. These variables were computed using the open-source web server ADMET lab 2.0. [40]. The supplementary data contains comprehensive analysis about the ADMET properties.

## Result and Discussion

### Density Functional Theory Calculations

The present study aimed to investigate the properties of a specific molecule using a combination of computational methods. The ground state structures were optimized using the B3LYP/SVP level of theory as implemented in the Gaussian 09W software, which is known for its high precision. Further calculations were performed on the optimized structures to determine key geometric parameters, electronic properties, and excited states. The

results of the frequency calculations confirmed that the optimized structures corresponded to true minima. Additionally, the optimized structures were obtained at  $-941.447687$  hartree in gas phase and  $-941.458041$  hartree in solvent phase, which can be seen in Fig. 2.

In order to understand the electronic properties of compounds, the B3LYP/SVP level of theory was utilized in the Gaussian 09W program to calculate the highest occupied molecular orbital (HOMO), the lowest unoccupied molecular orbital (LUMO), and the energy gap between them. These values are important indicators of a molecule's chemical activity, with the HOMO representing its ability to donate electrons and the LUMO representing its ability to accept electrons. A narrower energy gap between the HOMO and LUMO indicates a molecule that is more easily excited, while a wider gap indicates a molecule that is more stable. The DFT calculations for atropine revealed that it maintains a consistent energy gap in both gas and solvent phase, providing further insight into its unique properties as compared to other compounds. The results of these calculations can be found in Table 2.

The ability of a chemical compound to give or accept electrons is determined by its ionization potential ( $I$ ) and electron affinity ( $A$ ). These properties can be calculated by analyzing the energy difference between the highest occupied molecular orbital (HOMO) and the lowest unoccupied molecular orbital (LUMO). A small value for " $I$ " indicates that a compound is a strong electron donor, whereas a large value for " $A$ " indicates that a compound is a strong electron acceptor. In general, the energy difference between the HOMO and LUMO of soft molecules is relatively small. While the HOMO and LUMO energies do not directly correspond to the actual  $I$  and  $A$  values, there is a strong correlation between the HOMO energy and estimated  $I$  and the negative of the LUMO energy and measured  $A$ . As a result, the estimated HOMO and LUMO energies can be used to make semi-quantitative predictions of the ionization potential and electron affinity of a chemical compound.

In summary, the analysis of atropine's chemical properties using density functional theory (DFT) revealed that it has a low ionization potential in the gas phase, making it a strong electron donor. However, in the solvent phase, atropine has a greater electron affinity, indicating that it acts as a strong electron acceptor. Theoretical calculations were used to understand the potential anticancer activity of atropine by analyzing various properties such as electronegativity, chemical potential, hardness, softness, and electrophilicity index.

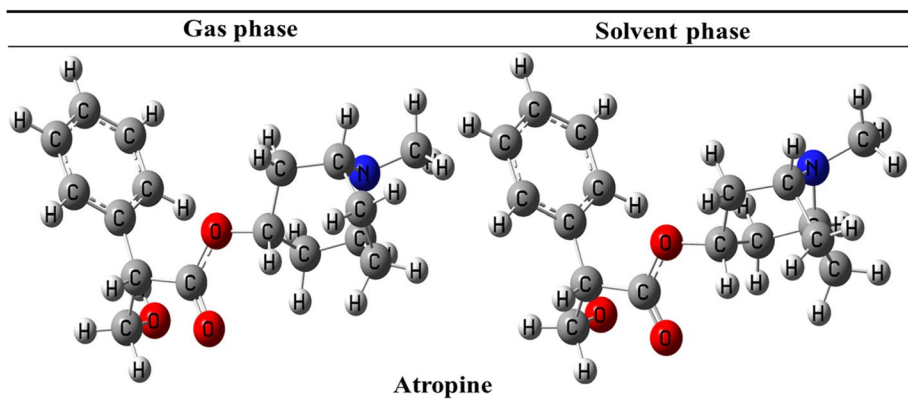


**Fig. 2** Optimized tropane alkaloid (atropine) structures in both the gas phase and the solvent phase

The electrophilicity index of atropine in the solvent phase was found to be high, suggesting that it behaves as a strong electrophile. All of these properties are listed in Tables 1 and 2, and it is important to note that chemical reactivity can vary depending on the structure of the molecule.

The molecular electrostatic potential (MEP) is a powerful tool for understanding the distribution of charge within a molecule and its chemical reactivity. By visualizing the relative polarity of a molecule, the MEP can provide insight into the size, shape, charge density, and chemical reactivity sites of the molecule. In this study, the MEP was calculated using DFT and the SVP basis set, as shown in Fig. 3. The three-dimensional charge distribution patterns were represented by an electron density isosurface mapped with an electrostatic potential surface. Different colors in Fig. 4 depict different electrostatic potential attributes, with red indicating the most electronegative regions, blue indicating the most positive regions, and green indicating regions with no electrostatic potential. An increase in ordered primary colors, from blue to red, indicates a stronger attraction or aversion to charge. Typically, negative potential zones are associated with electronegative lone pairs of atoms.

As illustrated in Fig. 3, the regions with a negative electrostatic potential are located around the TTF core and sulfur atom of the N-methylthiocarbamoyl group, whereas the regions with a positive electrostatic potential are located near the hydrogen atoms of alkyl and cyclic groups.

## Molecular Docking

Molecular docking is a computational technique that is widely used to predict the interaction between two molecules by creating a binding model. This technique is based on the molecular mechanics and molecular dynamics principles, which simulate the interactions between the small molecule (ligand) and the macromolecule (receptor). In current study, AKRB1 and AKRB10 were retrieved from protein data bank and subjected to evaluation against atropine via molecular docking approach. In this study, epalrestat was used as the standard drug and Nap was employed as a co-crystal ligand. The amino acid residues of active site for AKR1B1 and AKR1B10 were as follows: LEU 301, PHE 116, LEU 302, TRP 112, ASN 161, HIS 111, TRP 21, VAL 48, LEU 302, and TYR 210 for AKR1B10 whereas LEU 301, TRP 219, TRP 20, PHE 122, TRP 111, HIS 110, LEU 300, HIS 110, SER 302, and ALA 299 for AKR1B1 respectively. Notably, atropine exhibited stronger molecular interactions compared to the standard inhibitor. The binding energy of atropine against AKR1B1 and AKR1B10 was found to be  $-9.5$  and  $-9.3$  kcal/mol, respectively. This is in comparison to the binding

**Table 1** Energetic parameters of tropane alkaloid (atropine)

Compound	$E_{\text{HOMO}}$ (eV)	$E_{\text{LUMO}}$ (eV)	$\Delta E_{\text{gap}}$ (eV)	Potential ionization, $I$ (eV)	Affinity, $A$ (eV)
Gas phase					
Atropine	-0.217	-0.016	0.201	0.217	0.016
Solvent phase (water)					
Atropine	-0.219	-0.018	0.201	0.219	0.018

**Table 2** Quantum chemical descriptors of tropane alkaloid (atropine)

Gas phase Compound	Hardness ( $\eta$ )	Softness ( $S$ )	Electronegativity ( $X$ )	Chemical potential ( $\mu$ )	Electrophilicity index ( $\omega$ )
Atropine Compound	0.101 <b>Electron donating power</b> ( $\omega^+$ )	4.975	0.117 <b>Electron accepting power</b> ( $\omega^+$ )	-0.117	0.068 <b>Net Electrophilicity</b> ( $\Delta\omega^{\pm}$ )
Atropine	0.138		0.022		0.160
Solvent phase (water) Compound	Hardness ( $\eta$ )	Softness ( $S$ )	Electronegativity ( $X$ )	Chemical potential ( $\mu$ )	Electrophilicity index ( $\omega$ )
Atropine Compound	0.101 <b>Electron donating power</b> ( $\omega^+$ )	4.967	0.118 <b>Electron accepting power</b> ( $\omega^+$ )	-0.118	0.070 <b>Net electrophilicity</b> ( $\Delta\omega^{\pm}$ )
Atropine	0.142		0.023		0.165



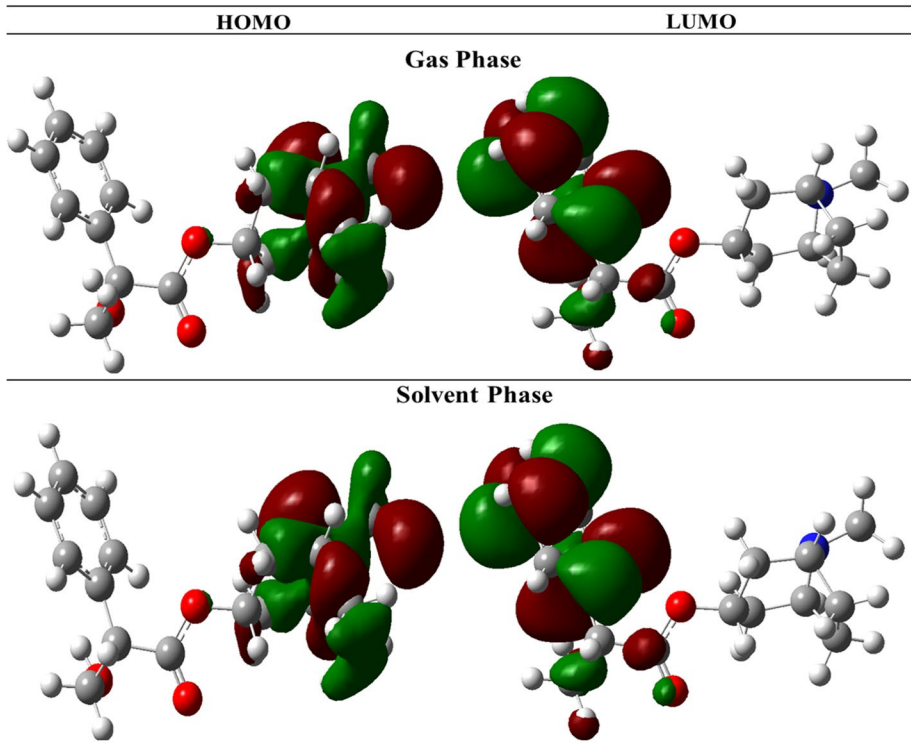


**Fig. 3** HOMO–LUMO structures of tropane alkaloid (atropine) in gas phase as well as in solvent phase

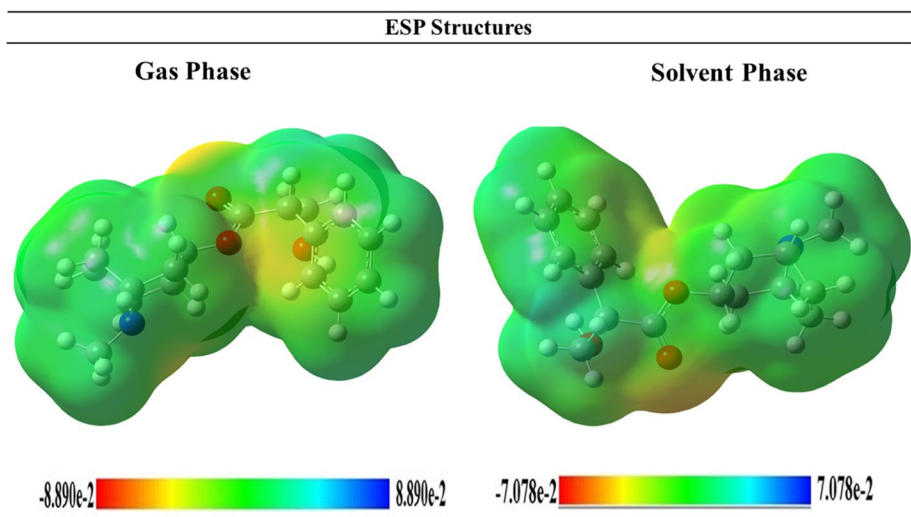


**Fig. 4** Showing MEP structures of tropane alkaloid (atropine) in gas phase as well as in solvent phase

energy of the standard inhibitor epalrestat against AKR1B1 and AKR1B10, which was determined to be  $-9.0$  and  $-8.7$  kcal/mol, respectively. These results suggest that atropine may have a greater potential as an inhibitor of AKR1B1 and AKR1B10 compared to the standard drug epalrestat. Table 3 is exhibiting the binding energies of selected compound against both proteins.

The study revealed that the molecular interactions of atropine against AKR1B1 were significant. Notably, atropine was found to produce two hydrogen bonds and one carbon-hydrogen bond with key amino acid residues in the active site of AKR1B1. In addition, several hydrophobic interactions were also observed to stabilize the protein–ligand complex. The amino acid residues of the active site of AKR1B1 involved in forming hydrogen bonds with atropine included LEU 300 and SER 302. A pi-donor hydrogen bond was formed by LEU 301. The amino acid residues involved in alkyl and pi-alkyl interactions included TRP 20, HIS 110, TRP 111, ALA 299, and the cofactor NAP 401. The binding energy of atropine against AKR1B1 was  $-9.5$  kcal/mol. These results suggest that atropine has a strong binding affinity for the active site of AKR1B1, potentially making it a more effective inhibitor of the enzyme compared to other compounds.

In terms of standard drug, it was notable that epalrestat was engaging TRP111, HIS110, TRP20, and NAP401 in hydrogen bonding. In addition, multiple cationic interactions were also stabilizing the complex. The binding energy of standard drug against AKR1B1 was  $-9.0$  kcal/mol. Figure 5 is illustrating presumed 2D and 3D interactions of atropine, NAP, and standard against AKR1B1.

The docked conformation of atropine against AKR1B10 revealed substantial interactions; however, these interactions were found to be less significant when compared to the interactions observed with AKR1B1. Notably, the amino acid residue of the active site of AKR1B10 that was involved in forming hydrogen bonds with atropine included TYR 110. Pi-Sigma interactions were observed with the amino acids TRP 20 and LEU 302, while Pi-Pi stacking was shown by TRP 112. Additionally, alkyl interactions were formed by the cofactor NAP 401. The binding energy of docked conformation was  $-9.3$  kcal/mol. These findings suggest that while atropine does have some binding potential with AKR1B10, it has a stronger binding affinity and inhibition potential towards AKR1B1.

The standard drug was also found to exhibit potential interactions with AKR1B10; however, these interactions were found to be inferior in number as only a single hydrogen bond was observed between the NH of HIS 111 and the electronegative oxygen atom of atropine. Additionally, several hydrophobic interactions were also observed to stabilize the complex. The docking score of the standard drug against AKR1B10 was determined to be  $-8.7$  kcal/mol. Figure 6 illustrates the proposed 2D and 3D interactions of atropine, NAP, and the standard drug against AKR1B10, respectively. These results suggest that while the standard drug does have some binding potential with AKR1B10, atropine has a stronger binding affinity and inhibition potential towards AKR1B10.

**Table 3** Binding energies of atropine with target proteins, i.e., AKR1B1 and AKR1B10 (kcal/mol)

Compound	AKR1B1 (kcal/mol)	AKR1B10 (kcal/mol)
Atropine	$-9.5$	$-9.3$
Co-crystal (NAP)	$-10.4$	$-10.1$
Epalrestat inhibitor	$-9.0$	$-8.7$

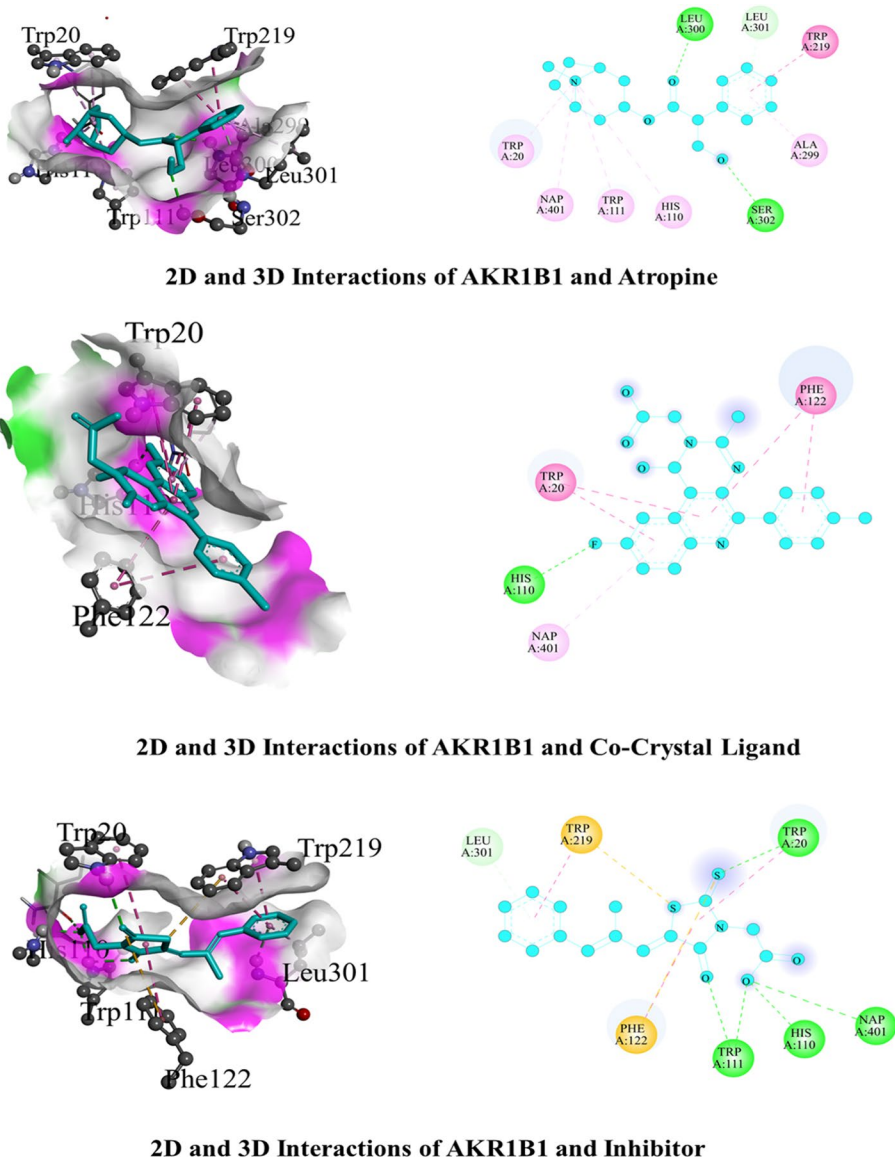


**Fig. 5** Showing 3D and 2D interactions of tropane alkaloid (atropine), co-crystal ligand, and standard inhibitor with active site of AKR1B1

The results of the docking analysis and comparison of binding energies have confirmed that atropine has a greater potential for inhibiting both AKR1B1 and AKR1B10 compared to the standard inhibitor. Furthermore, it was observed that the inhibition potential of atropine towards AKR1B1 is relatively stronger when compared to AKR1B10. These findings suggest that atropine may be a promising

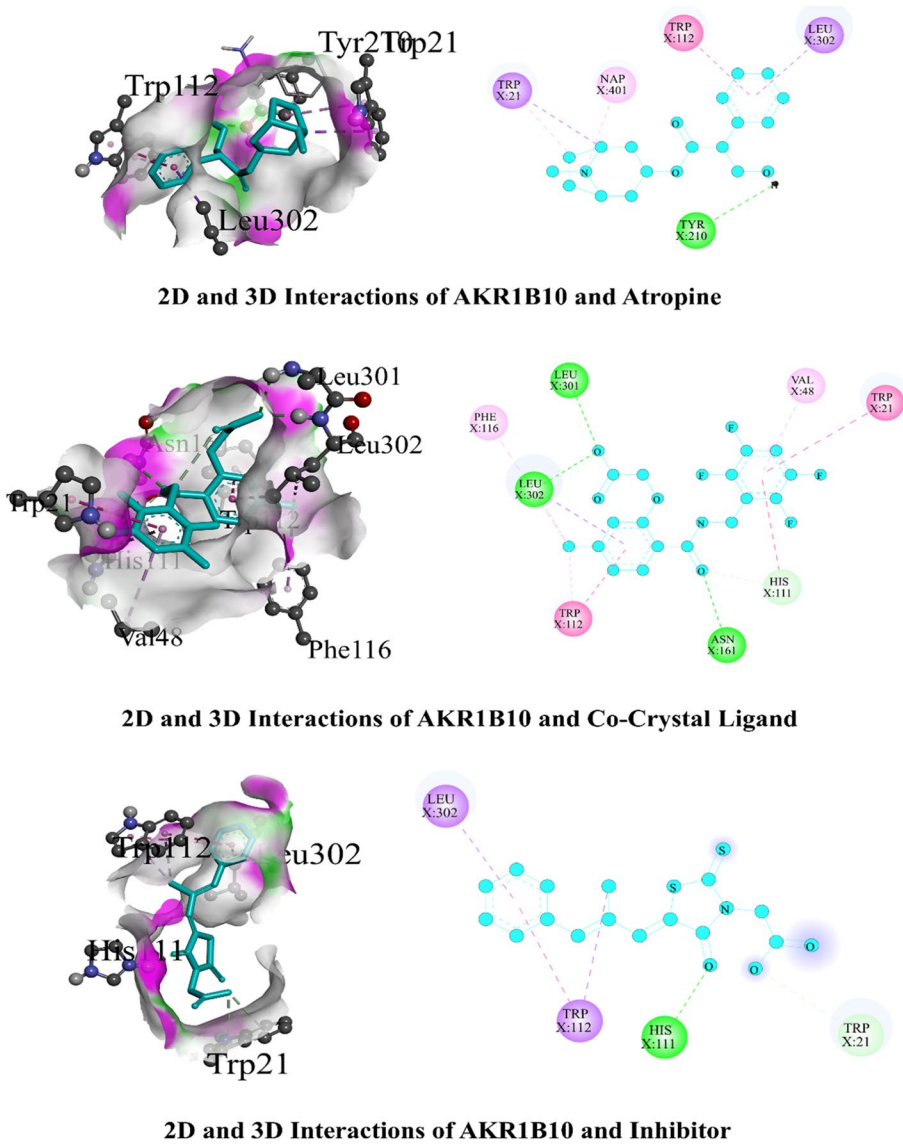


**Fig. 6** Showing 2D and 3D interactions of tropane alkaloid (atropine), co-crystal ligand, and standard inhibitor with active site of AKR1B10

candidate for the development of new drugs for the treatment of conditions associated with the overexpression of AKR1B1 and AKR1B10.

**Molecular Dynamic Simulations**

Molecular dynamics (MD) simulations were used to evaluate the stability and interactions of the protein–ligand complex. The RMSD, RMSF, and other parameters were analyzed

during the simulation to gain a deeper understanding of the structural changes within the protein. The RMSD, which is calculated by comparing the protein structure at each point in the simulation to a reference frame, can be used to assess the overall stability of the protein over time. Additionally, this analysis can be used to determine if the final structure of the simulation is close to a thermal average structure. It is important to note that for small and globular proteins, RMSD values of 1–3 are considered to be within an acceptable range [35].

The stability of the protein–ligand complexes of atropine with AKR1B1 and AKR1B10 was analyzed using the root mean square deviation (RMSD) method. The RMSD values were calculated by aligning the protein–ligand complex on the reference protein backbone, as shown in Fig. 7. The results showed that the RMSD values for the atropine–protein complexes were within the acceptable range, indicating that the ligand remained in its binding site throughout the simulation. The RMSD values were also compared to the RMSD values of the standard drug, epalrestat, in complex with AKR1B1 and AKR1B10, to determine the stability of the atropine complexes in relation to the standard drug.

The stability of the protein–ligand complex was evaluated using the root mean square deviation (RMSD) of the C-alpha atoms of the apoprotein. Figure 7 illustrates the evolution of the RMSD over time. The RMSD plot of the AKR1B1–atropine complex indicates that stability is achieved after 45 ns, while the AKR1B10–atropine complex indicates that stability is achieved after 35 ns. The RMSD fluctuations for the complex remained near 2.0 Å throughout the simulation, which is considered acceptable. After equilibration, the RMSD values between the ligands and proteins fluctuated within 1.5 Å. Between 25 and 40 ns, the RMSD values were slightly larger for the AKR1B1–atropine complex. The simulation results indicate that the ligands were tightly bound to the receptor’s binding site and that the complexes were stable over the course of the simulation. This suggests that atropine has a strong binding affinity towards AKR1B1 and AKR1B10 and is able to form stable complexes with these enzymes.

The RMSD pattern of standard epalrestat with both proteins demonstrated significant stability. The protein–ligand complex achieved stability immediately after the initiation of the MD simulations. However, initially slight fluctuations were observed which indicate the rearrangements of epalrestat inside the active pocket of the protein. The RMSD of epalrestat–AKR1B1 complexes ranges from 2 to 3.6 Å, which indicate the potential inhibitory mechanism of the standard drug. Additionally, the RMSD of epalrestat–AKR1B10 was

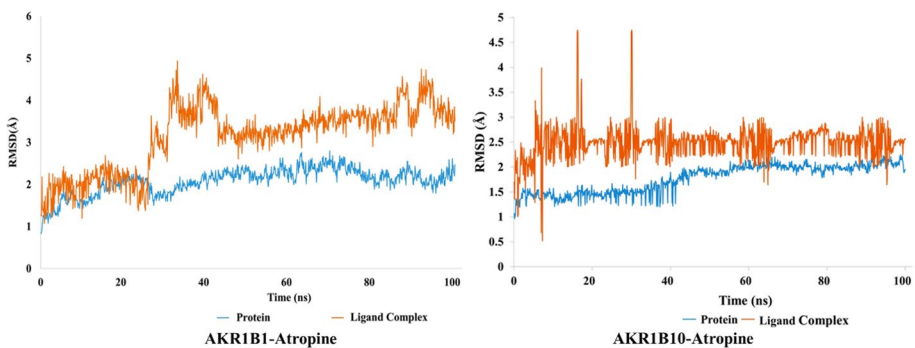


**Fig. 7** RMSD of the AKR1B1–atropine and AKR1B10 atropine complex with time. The protein RMSD’s variation is displayed on the left Y-axis. The ligand RMSD’s variation is displayed on the right Y-axis

equilibrated around 3.5 Å. These findings indicate that the stability of the atropine complex with targeted proteins was comparable to that of the standard inhibitor epalrestat. In conclusion, it can be inferred that atropine has a similar inhibitory potential as that of the standard drug epalrestat. Figure 8 illustrates the RMSD pattern of the standard drug in complex with both proteins.

The stability and conformation of the protein–ligand complex were analyzed using secondary structural elements (SSE) such as beta strands and alpha helices throughout the simulation, as illustrated in Fig. 9. The distribution of SSE by residue index throughout the protein structure is depicted in the graph, where the bottom plot shows the SSE assignment for each residue over time, and the top image illustrates the SSE composition for each frame of the simulation. These findings provide a deeper understanding of how the binding of the ligand affects the structure of the protein and how it preserves the protein's native conformation. The SSE analysis confirms the stability of the protein–ligand complex, giving insights into the structural basis of the inhibition of AKR1B1 and AKR1B10 by atropine.

Molecular Mechanics Poisson-Boltzmann Surface Area (MMPBSA) analysis was performed for all four complexes. It is an efficient approach to take into account all the electrostatic interactions, Coulomb interactions, and polar and nonpolar energies existed between the protein–ligand complex. In the current study, a comparative analysis of the standard epalrestat and atropine was performed. Both drugs exhibited comparable binding energies. However, atropine's binding free energies were better than the standard drug epalrestat. This suggests that atropine has a stronger binding affinity towards AKR1B1 and AKR1B10 than epalrestat, making it a more potent inhibitor of these enzymes. These findings provide a deeper understanding of the binding mechanism of atropine and the potential it holds for the treatment of colon cancer associated with the overexpression of AKR1B1. The following equation was used to integrate MMPBSA analysis:

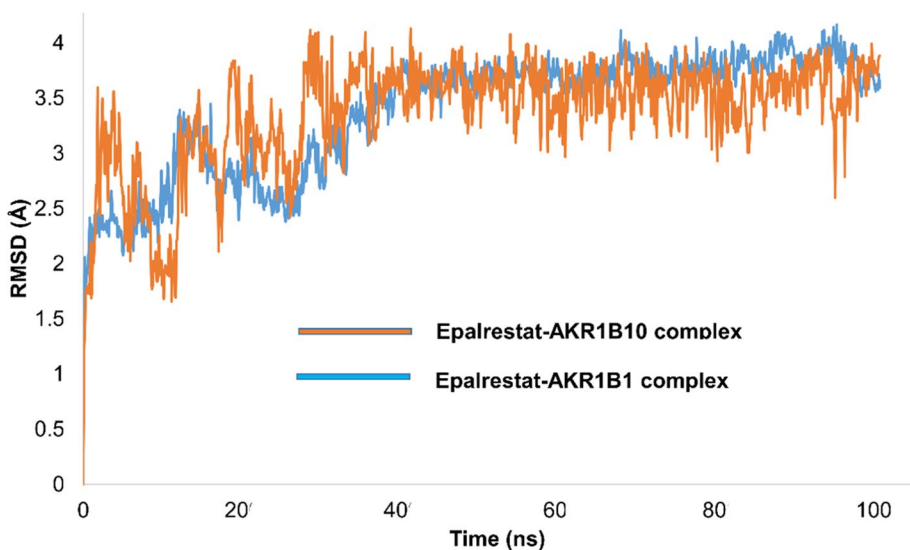


**Fig. 8** Evolution of RMSD for epalrestat-AKR1B1 complex (blue colored trajectory) and epalrestat-AKR1B10 complex (orange colored trajectory)

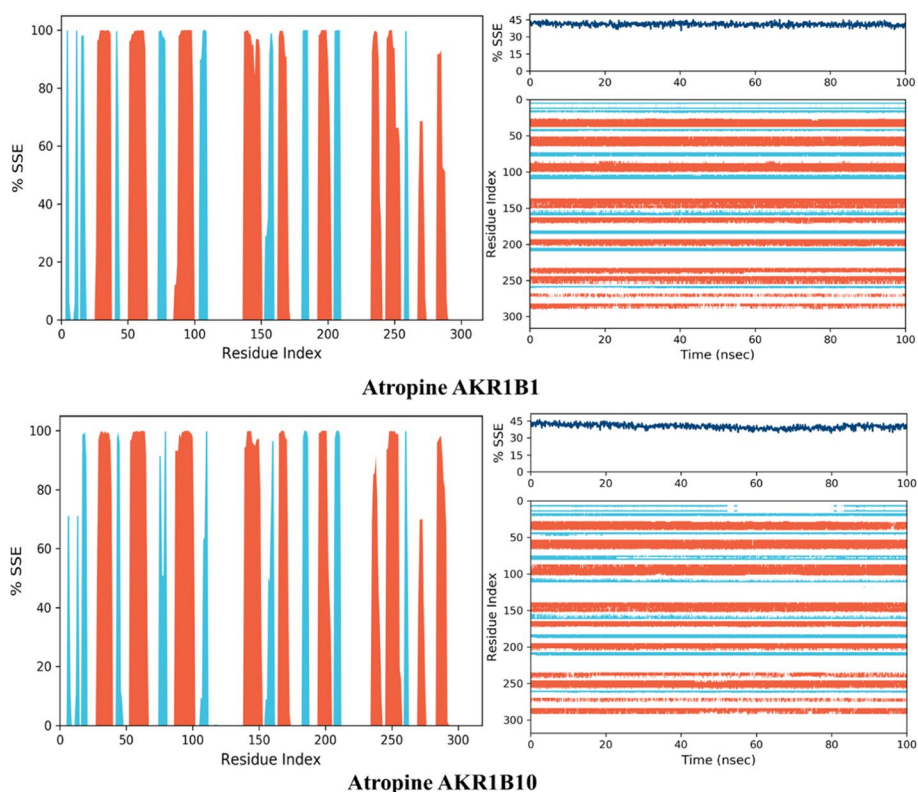


**Fig. 9** In the entire protein structure, AKR1B1 and AKR1B10 were bound with the atropine secondary structure element distribution by residue index. Alpha helices are denoted in red, and beta strands are denoted in blue

**Table 4** MMPBSA binding free energy analysis

Complex	Binding free energies (kcal/mol)	$E_{\text{electrostatic}}$ (kcal/mol)	$\Delta E_{\text{vdW}}$ (kcal/mol)	$E_{\text{Npolar}}$ (kcal/mol)
Atropine-AKR1B1	-69.43	-24.3	-40.6	-19.2
Atropine-AKR1B10	-60.44	-25.11	-30.5	-23.2
Epalrestat-AKR1B1	-58.32	-19.5	-44.9	-11.9
Epalrestat-AKR1B10	-50.98	-33.2	-25.2	-17.5

$$G = E_{\text{bind}} + E_{\text{el}} + E_{\text{vdW}} + G_{\text{pol}} + G_{\text{np}} - \text{TS.}$$

Table 4 is indicating the MMPBSA free binding energies for all four complexes.

## ADMET Properties and Toxicity Profile

The solubility and absorption of a compound can be determined by analyzing its LogP and LogS values. Atropine is lipophilic, which means it has a higher LogP value,

indicating that it is not very hydrophilic. The LogS value, which measures solubility, should be low for optimal absorption. For drugs that target the central nervous system, the ideal lipophilicity for crossing the blood–brain barrier is a LogD of 2 or less. A LogD value above 4 is typically not suitable for CNS drugs. The topological polar surface area (TPSA) can also be calculated to predict oral absorption. A lower TPSA value is preferred as it indicates better membrane permeability. A compound is considered to have good bioavailability if it has a TPSA of 70 or less. The number of hydrogen bond donors (nHD) and acceptors (nHA) can also be used to assess the compound's suitability for drug development. Optimal ranges for nHD and nHA are between 0 and 12 and 0 and 7 respectively (Table 5).

In terms of its ability to be absorbed and distributed in the body, atropine was found to have a high HIA value, indicating that it will be readily absorbed from the gastrointestinal tract. This results in an increased blood plasma concentration of the compound. Additionally, the calculated BBB value indicated that atropine is able to easily pass across the blood–brain barrier due to its natural lipophilicity. It was also found to have moderate binding to plasma proteins, and its volume of distribution was within the optimal range of 0.04–20 L/kg. In vitro testing using the Caco-2 cell monolayer model also revealed that atropine has a high level of intestinal permeability, with a value greater than  $-5.15$  log units (Table 6).

The permeability of atropine was studied using MDCK cells, which are commonly used to investigate drug efflux and active transport mechanisms, such as P-glycoprotein efflux. The results showed that atropine has a low to moderate permeability in these cells. A low permeability is considered to be less than 2, medium permeability is between 2 and 20, and high permeability is greater than 20. Additionally, the clearance rate of atropine was also evaluated and found to be good, which is categorized as high ( $> 15$ ), moderate (5–15), or low (less than 5). Overall, the results suggest that atropine has a favorable drug efflux and active transport profile (Table 7).

The potential mutagenicity of atropine was evaluated using the AMES toxicity test, and the results indicated that it is not carcinogenic. Additionally, the ease of synthesis for atropine was determined using the synthetic accessibility score (SAscore), which revealed that it is relatively simple to produce. Furthermore, a toxicity profile assessment was conducted and it was found that the compound has a low toxicity risk and does not pose significant risk for corrosion or eye irritation. It also has a low potential for carcinogenic and respiratory toxicity (Table 8).

The androgen receptor (AR) and estrogen receptor (ER) activity of atropine was analyzed using NR-AR and NR-ER tests, respectively. The results showed that atropine acted as an activator for both receptors. In addition, the antioxidant response element (ARE) activity of atropine was also analyzed using SR-ARE test, which revealed that atropine acted as an activator (Table 9). These findings suggest that atropine has the potential to activate certain receptors in the body.

**Table 5** Physicochemical properties of tropane alkaloid (atropine)

Physicochemical properties								
	Molecular weight	Density	nHA	nHD	TPSA	LogS	LogP	LogD
Atropine	289.17	0.952	4	1	49.77	-2.033	1.877	1.315



**Table 6** Absorption and distribution properties of the tropane alkaloid (atropine)

Absorption and distribution properties								
Codes	Volume of distribution	Human intestinal absorption	Caco-2 permeability	Blood–brain barrier and blood-placenta barrier	Plasma protein binding	Pgp inhibitor	P-glycoprotein substrate	MDCK permeability
Atropine	2.461	0.03	– 4.885	0.263	29.68%	0.001	0.064	5e-05

**Table 7** Metabolism and excretion values of tropane alkaloid (atropine)

Metabolism	Excretion					
	CYP1A2 inhibitor	CYP2C19 inhibitor	CYP2C9 inhibitor	CYP2D6 inhibitor	CYP3A4 inhibitor	T1/2
Atropine	0.024	0.027	0.012	0.834	0.04	10.3
						0.215

**Table 8** Medicinal properties and toxicity profile of tropane alkaloid (atropine)

Codes	Medicinal properties		Toxicity				
	Synthetic accessibility score	Lipinski rule	AMES toxicity	Carcinogenicity	Eye corrosion	Eye irritation	Respiratory toxicity
Atropine	3.937	Accepted	0.037	0.086	0.003	0.01	0.74

**Table 9** Various toxicological parameters of tropane alkaloid (atropine)

Tox21 pathway				
	NR-AR	NR-AR-LBD	NR-ER	Antioxidant response element
Atropine	0.024	0.002	0.495	0.064

## Conclusion

In conclusion, the present study has identified atropine as a promising inhibitor of AKR1B1, an enzyme known to play a key role in the development of colon cancer and related malignancies. Through the use of advanced computational techniques such as DFT calculations, molecular docking, and molecular dynamics simulations, it was found that atropine selectively targets AKR1B1 over AKR1B10, and has a greater inhibition potential towards AKR1B1 than the standard inhibitor epalrestat. These findings provide a deeper understanding of the binding mechanism of atropine and the potential it holds for the treatment of colon cancer associated with the overexpression of AKR1B1. Furthermore, the results of the ADMET analysis and toxicity profile suggest that further derivatization of atropine may lead to the development of more potent and effective anti-cancer compounds. The potential of atropine as a repurposed drug for cancer therapy is a promising avenue for future research. As atropine is already an FDA-approved drug, this repurposing will open new doors of research to tackle the challenge of a wide variety of carcinomas.

**Supplementary Information** The online version contains supplementary material available at <https://doi.org/10.1007/s12010-023-04411-2>.

**Author Contribution** S.A.E. and G.S.B. devised and supervised the study plan. S.A.E., S.S.A., M.A., and F.S. carried out the molecular docking investigations and DFTs. The MD simulations were performed by S.A.E and M.A. The manuscript write up was carried out by S.A.E., G.S.B., A.A., and S.M.A. All authors read and approved the manuscript for publication.

**Funding** This study was supported by Taif University Researchers supporting project (number TURSP-2020/38), Taif University, Taif, Saudi Arabia, for research resources.

**Data Availability** All data generated or analyzed during this study are included in this article (and its supplementary information file).

## Declarations

**Ethics Approval** Not applicable

**Consent to Participate** All authors were agreed to participate.

**Consent for Publication** All authors have approved the last version of the manuscript for its submission.

**Conflict of Interest** The authors declare no competing interests.

## References

- Chen, J., & Huang, X.-F. (2009). The signal pathways in azoxymethane-induced colon cancer and preventive implications. *Cancer biology & therapy*, 8(14), 1313–1317.
- Bauer, B., et al. (2020). Quantum algorithms for quantum chemistry and quantum materials science. *Chemical Reviews*, 120(22), 12685–12717.


3. Chen, J., & Huang, X.-F. (2009). The signal pathways in azoxymethane-induced colon cancer and preventive implications. *Cancer biology therapy*, 8(14), 1313–1317.
4. Matsunaga, T., et al. (2012). Aldo–keto reductase 1B10 and its role in proliferation capacity of drug-resistant cancers. *Frontiers in pharmacology*, 3, 5.
5. Ruiz, F. X., et al. (2011). Human and rodent aldo–keto reductases from the AKR1B subfamily and their specificity with retinaldehyde. *Chemico-biological interactions*, 191(1–3), 199–205.
6. Demirkol Canlı, S., et al. (2020). Evaluation of an aldo-keto reductase gene signature with prognostic significance in colon cancer via activation of epithelial to mesenchymal transition and the p70S6K pathway. *Carcinogenesis*, 41(9), 1219–1228.
7. Alam, M., et al. (2018). DFT/TD-DFT calculations, spectroscopic characterizations (FTIR, NMR, UV–vis), molecular docking and enzyme inhibition study of 7-benzoyloxycoumarin. *Computational Biology Chemistry*, 73, 65–78.
8. Kaur, R., & Arora, S. (2015). Alkaloids-important therapeutic secondary metabolites of plant origin. *Critical Review*, 2(3), 1–8.
9. Devi, R., et al. (2020). Fungal secondary metabolites and their biotechnological applications for human health. *New and future developments in microbial biotechnology and bioengineering* (pp. 147–161). Elsevier.
10. Kaur, R., & Arora, S. (2015). Alkaloids-important therapeutic secondary metabolites of plant origin. *J Crit Rev*, 2(3), 1–8.
11. Gryniewicz, G., & Gadzikowska, M. (2008). Tropane alkaloids as medicinally useful natural products and their synthetic derivatives as new drugs. *Pharmacological Reports*, 60(4), 439.
12. Kohnen-Johannsen, K. L., & Kayser, O. (2019). Tropane alkaloids: Chemistry, pharmacology, biosynthesis and production. *Molecules*, 24(4), 796.
13. Hallcher, L. M., & Sherman, W. R. (1980). The effects of lithium ion and other agents on the activity of myo-inositol-1-phosphatase from bovine brain. *Journal of Biological Chemistry*, 255(22), 10896–10901.
14. Mohanlall, V., & Ally, F. (2020). An overview of tropane alkaloids from *Datura stramonium* L. *Journal of Pharmacognosy Phytochemistry*, 9(3), 5–13.
15. Prieto-Martínez, F. D., Arciniaga, M., & Medina-Franco, J. L. (2018). Molecular docking: Current advances and challenges. *TIP. Revista especializada en ciencias químico-biológicas*, 21(1), 65–87.
16. Rasheed, M. A., et al. (2021). Identification of lead compounds against Scm (fms10) in *Enterococcus faecium* using computer aided drug designing. *Life*, 11(2), 77.
17. Alam, M., et al. (2018). DFT/TD-DFT calculations, spectroscopic characterizations (FTIR, NMR, UV–vis), molecular docking and enzyme inhibition study of 7-benzoyloxycoumarin. *Computational Biology and Chemistry*, 73, 65–78.
18. Frisch, M., et al. (2003). *Revision B. Gaussian 03*. Gaussian Inc., Pittsburgh (PA).
19. Goerigk, L., & Reimers, J. R. (2013). Efficient methods for the quantum chemical treatment of protein structures: The effects of London-dispersion and basis-set incompleteness on peptide and water-cluster geometries. *Journal of Chemical Theory Computation*, 9(7), 3240–3251.
20. Tirado-Rives, J., & Jorgensen, W. L. (2008). Performance of B3LYP density functional methods for a large set of organic molecules. *Journal of chemical theory computation*, 4(2), 297–306.
21. Dennington, R., Keith, T. A. & Millam, J. M. (2016). *GaussView, version 6.0*. 16. Semichem Inc Shawnee Mission KS, USA.
22. Torres, J. A. G., et al. (2019). Low-scaling algorithm for nudged elastic band calculations using a surrogate machine learning model. *Physical review letters*, 122(15), 156001.
23. Dennington, R., Keith, T.A. & Millam, J. M. (2016). *GaussView 6.0*. 16. Semichem Inc.
24. Channar S. A., et al., (2022). Exploring thiazole-linked thioureas using alkaline phosphatase assay, biochemical evaluation, computational analysis and structure–activity relationship (SAR) studies. *Medicinal Chemistry Research*, 31(10), 1792–802.
25. Aziz, M., et al. (2022). Identification of potent inhibitors of NEK7 protein using a comprehensive computational approach. *Scientific reports*, 12(1), 1–17.
26. Berman, H., Henrick, K., & Nakamura, H. (2003). Announcing the worldwide protein data bank. *Nature Structural Molecular Biology*, 10(12), 980–980.
27. Morris, G. M., et al. (2009). AutoDock4 and AutoDockTools4: Automated docking with selective receptor flexibility. *Journal of computational chemistry*, 30(16), 2785–2791.
28. Trot, O., & Olson, A. J. (2010). AutoDock Vina: Improving the speed and accuracy of docking with a new scoring function, efficient optimization, and multithreading. *Journal of computational chemistry*, 31(2), 455–461.
29. Belhassan, A., et al. (2021). Camphor, artemisinin and sumac phytochemicals as inhibitors against COVID-19: Computational approach. *Computers in Biology Medicine*, 136, 104758.

30. Ouassaf, M., et al. (2021). Combined docking methods and molecular dynamics to identify effective antiviral 2, 5-diaminobenzophenone derivatives against SARS-CoV-2. *Journal of King Saud University-Science*, 33(2), 101352.
31. Morris, G. M., et al. (1998). Automated docking using a Lamarckian genetic algorithm and an empirical binding free energy function. *Journal of computational chemistry*, 19(14), 1639–1662.
32. Heinzerling, L., Klein, R., & Rarey, M. (2012). Fast force field-based optimization of protein–ligand complexes with graphics processor. *Journal of Computational Chemistry*, 33(32), 2554–2565.
33. Visualizer, Discovery Studio. Accelrys software inc. Discovery studio visualizer 2.
34. Wang, Z., et al. (2016). Comprehensive evaluation of ten docking programs on a diverse set of protein–ligand complexes: The prediction accuracy of sampling power and scoring power. *Physical Chemistry Chemical Physics*, 18(18), 12964–12975.
35. Aziz, M., et al. (2022). Identification of NEK7 inhibitors: Structure based virtual screening, molecular docking, density functional theory calculations and molecular dynamics simulations. *Journal of Biomolecular Structure Dynamics*, 1–15.
36. Bowers, K. J., et al. (2006). Scalable algorithms for molecular dynamics simulations on commodity clusters. In *SC'06: Proceedings of the 2006 ACM/IEEE Conference on Supercomputing*. 84.
37. Ferreira, L. G., et al. (2015). Molecular docking and structure-based drug design strategies. *Molecules*, 20(7), 13384–13421.
38. Belhassan, A., et al. (2022). In silico detection of potential inhibitors from vitamins and their derivatives compounds against SARS-CoV-2 main protease by using molecular docking, molecular dynamic simulation and ADMET profiling. *Journal of molecular structure*, 1258, 132652.
39. Channar, P. A., et al. (2021). Structural and functional insight into thiazolidinone derivatives as novel candidates for anticancer drug design: In vitro biological and in-silico strategies. *Journal of Biomolecular Structure Dynamics*, 1–12.
40. Xiong, G., et al. (2021). ADMETlab 2.0: An integrated online platform for accurate and comprehensive predictions of ADMET properties. *Nucleic Acids Research*, 49(W1), W5–W14.

**Publisher's Note** Springer Nature remains neutral with regard to jurisdictional claims in published maps and institutional affiliations.

Springer Nature or its licensor (e.g. a society or other partner) holds exclusive rights to this article under a publishing agreement with the author(s) or other rightsholder(s); author self-archiving of the accepted manuscript version of this article is solely governed by the terms of such publishing agreement and applicable law.

## Authors and Affiliations

Syeda Abida Ejaz<sup>1</sup>  · Mubashir Aziz<sup>1</sup> · Aftab Ahmed<sup>1</sup> · Saqer S. Alotaibi<sup>2</sup> · Sarah M. Albogami<sup>2</sup> · Farhan Siddique<sup>3,4</sup> · Gaber El-Saber Batiha<sup>5</sup>

<sup>1</sup> Department of Pharmaceutical Chemistry, Faculty of Pharmacy, The Islamia University of Bahawalpur, Bahawalpur 63100, Pakistan

<sup>2</sup> Department of Biotechnology, College of Science, Taif University, P.O. Box 11099, Taif 21944, Saudi Arabia

<sup>3</sup> Laboratory of Organic Electronics, Department of Science and Technology, Linköping University, 60174 Norrköping, Sweden

<sup>4</sup> Department of Pharmaceutical Chemistry, Faculty of Pharmacy, Bahaiddian Zakariya University, Multan 60800, Pakistan

<sup>5</sup> Department of Pharmacology and Therapeutics, Faculty of Veterinary Medicine, Damanhour University, Damanhour 22511, AlBeheira, Egypt